Mon. Not. R. Astron. Soc. **000**, 000–000 (1995)

# The Cambridge-Cambridge ROSAT Serendipity Survey – V: Catalogue and Optical Identifications

B.J.Boyle[1], B.J.Wilkes[2], M.Elvis[2]

[1] *Royal Greenwich Observatory, Madingley Road, Cambridge, CB3 0EZ*
[2] *Harvard-Smithsonian Center for Astrophysics, 60 Garden St, Cambridge, MA 02138, USA.*

**ABSTRACT**
We report the results of a medium-depth X-ray survey of 20 *ROSAT* PSPC fields. 123 X-ray sources were detected down to a flux limit of $S(0.5-2\,\mathrm{keV}) > 2\times 10^{-14}\,\mathrm{erg\,s^{-1}\,cm^{-2}}$ lying between that of the *Einstein* Extended Medium Sensitivity Survey and the deepest *ROSAT* surveys. Optical identifications of 110 of these sources have revealed 68 QSOs, 12 NLXGs, 24 stars, 2 BL Lac objects, 2 galaxies and two clusters. CCD imaging reveals the possible presence of galaxy groups or clusters at the positions of a further 4 X-ray sources. The number-redshift and $\log N - \log S$ relations of the 68 QSOs are in better agreement with the faster rate of cosmological evolution for X-ray QSOs derived from *ROSAT* deep surveys ($L_X \propto (1+z)^{3.34\pm0.1}$, $z_{\max} = 1.79$) than with the evolution obtained from the EMSS ($L_X \propto (1+z)^{2.55\pm0.1}$), the latter being rejected at greater than the $3\sigma$ level as a model for the current sample. We present the optical spectra and measurements of the emission lines. The equivalent width distributions are consistent with those of QSO samples selected in other wavebands. We find no evidence for an inverse correlation between line width and X-ray spectral slope as recently reported for other *ROSAT* QSO samples.

**Key words:** X-rays: general – galaxies: active – quasars: general

## 1 INTRODUCTION

The high sensitivity of the *ROSAT* PSPC has allowed a number of X-ray surveys to be made to significantly fainter flux levels than was previously possible (e.g. Shanks et al. 1991, Hasinger et al. 1993, Branduardi-Raymont et al. 1994), shedding new light on the nature of faint X-ray sources and their cosmological evolution. Results from one deep *ROSAT* survey (Boyle et al. 1994) have previously implied significantly faster QSO evolution than had been deduced from earlier surveys at somewhat higher energies such as the *Einstein* Medium Sensitivity Survey (Maccacaro et al. 1991). This discrepancy is not well understood, possible explanations include the different energy ranges of the *Einstein* IPC (0.3–3.5 keV) and *ROSAT* PSPC (0.5–2 keV), which can result in different spectral components dominating the QSO X-ray spectra (see Ciliegi et al. 1995), and the inclusion of the redshift cut-off in the modelling procedure (Jones et al. 1996).

However, the EMSS and *ROSAT* deep survey also have different characteristics. This can be seen from the X-ray luminosity-redshift diagram for QSOs selected from the two samples (Fig. 1). There is little or no overlap between the distribution of QSO X-ray luminosities at a given redshift in the two surveys and thus they are sampling different parts of the QSO population. In an attempt to fill in the gap in the luminosity-redshift plane between these two surveys, we made a survey of 20 medium-depth (5000 – 30000 sec) PSPC observations (the Cambridge-Cambridge *ROSAT* serendipity survey, CRSS). The resulting sample, with a flux limit between the EMSS ($S(0.3-3.5\,\mathrm{keV}) > 1\times10^{-13}\,\mathrm{erg\,s^{-1}\,cm^{-2}}$, Gioia et al. 1990) and the *ROSAT* deep survey ($S(0.5-2\,\mathrm{keV}) > 4\times10^{-15}\,\mathrm{erg\,s^{-1}\,cm^{-2}}$, Boyle et al. 1994), results in continuous coverage of the L,z plane and overlaps with both the other samples, facilitating a significantly improved comparison between the samples (see Fig. 1). Other X-ray samples currently near completion, e.g. the *ROSAT* International X-ray Optical Survey (RIXOS, see Page et al. 1996) will also help to fill this important gap.

In this paper we report the X-ray source positions and fluxes, the optical identifications and make a comparison between this survey and the EMSS and *ROSAT* deep surveys discussed above. In associated papers we also discuss the nature of the significant subset of narrow emission-line X-ray-luminous galaxies (NLXGs) found in this sample (Boyle et al. 1995a: Paper I, Boyle et al. 1995b: Paper II), the X-ray spectral properties of the QSOs in the sample (Ciliegi et al. 1996, Paper IV), and the radio fluxes of the sample (Ciliegi et al. 1995, Paper III).

## 2 OBSERVATIONS

### 2.1 X-ray source detection

**Table 1.** Survey Fields

| Field Name | RA (J2000) h m s | Dec ° ′ ″ | Flux Limit† ($\mathrm{erg\,s^{-1}\,cm^{-2}}$) | $N_H$ ($10^{20}\,\mathrm{cm^{-2}}$) | ROR# | Date | PSPC | Exp.Time (sec) | # srcs† | POSS field |
|---|---|---|---|---|---|---|---|---|---|---|
| MKN335 | 00 08 19.2 | 20 41 24 | $2.0 \times 10^{-14}$ | 4.1 | 700101 | 1991 June 29-30 | B | 24586 | 10 | EO1195 |
| PG0027 | 00 30 05.7 | 26 17 22 | $2.0 \times 10^{-14}$ | 3.9 | 300016 | 1991 July 4-5 | B | 26676 | 7 | EO1188 |
| OQ208 | 14 07 00.4 | 28 27 14 | $2.0 \times 10^{-14}$ | 1.4 | 700061 | 1991 July 12-13 | B | 26050 | 10 | EO86 |
| PG1411 | 14 13 48.4 | 44 00 14 | $2.0 \times 10^{-14}$ | 1.2 | 700248 | 1991 June 26-27 | B | 25319 | 9 | EO1386 |
| Q1413+11 | 14 15 46.3 | 11 29 44 | $2.0 \times 10^{-14}$ | 1.8 | 700122 | 1991 July 20-21 | B | 28066 | 19 | EO1051 |
| 3C298 | 14 19 08.2 | 06 28 35 | $2.0 \times 10^{-13}$ | 2.1 | 700865 | 1992 July 25-Aug 6 | B | 10714 | 1 | EO1418 |
| | | | | | | 1993 Jan 12 | B | 8884 | | |
| OQ530 | 14 19 46.6 | 54 23 14 | $2.0 \times 10^{-14}$ | 1.3 | 150046 | 1990 July 19-22 | C | 11516 | 8 | EO1409 |
| 4U1417+42 | 14 28 32.5 | 42 40 25 | $3.0 \times 10^{-14}$ | 1.4 | 700535 | 1992 Jan 24 | B | 9593 | 5 | EO145 |
| PG1426 | 14 29 06.6 | 01 17 06 | $2.5 \times 10^{-14}$ | 2.7 | 150007 | 1990 July 18-19 | C | 6485 | 4 | EO1440 |
| PG1512 | 15 14 43.0 | 36 50 51 | $4.0 \times 10^{-14}$ | 1.4 | 700807 | 1992 Aug 12-17 | B | 5230 | 5 | EO1610 |
| NGC5907 | 15 15 52.9 | 56 19 33 | $2.0 \times 10^{-14}$ | 1.4 | 600190 | 1992 Jan 6-13 | B | 18164 | 9 | EO1096 |
| PG1543 | 15 45 30.1 | 48 46 12 | $3.0 \times 10^{-14}$ | 1.6 | 700808 | 1992 Aug 22-23 | B | 7181 | 5 | EO1404 |
| | | | | | 700809 | 1992 Aug 21-22 | B | 5578 | | |
| MS1603.6 | 16 05 46.0 | 25 51 44 | $2.0 \times 10^{-14}$ | 4.6 | 300021 | 1991 Aug 26 | B | 24845 | 7 | EO113 |
| E1615+061 | 16 17 45.5 | 06 03 55 | $3.5 \times 10^{-14}$ | 4.6 | 700213 | 1991 Feb 19-20 | B | 11427 | 2 | EO1067 |
| 3C334 | 16 20 21.8 | 17 36 22 | $5.0 \times 10^{-14}$ | 4.1 | 700274 | 1991 Mar 5-6 | B | 15722 | 1 | EO55 |
| MKN501 | 16 53 52.2 | 39 45 36 | $7.5 \times 10^{-14}$ | 1.7 | 700130 | 1991 Feb 25-26 | B | 7649 | 2 | EO1135 |
| PG1704 | 17 04 41.5 | 60 44 28 | $2.0 \times 10^{-14}$ | 2.3 | 700439 | 1991 Oct 28-30 | B | 13068 | 8 | EO1414 |
| PG2233 | 22 36 07.7 | 13 43 55 | $5.0 \times 10^{-14}$ | 4.9 | 700438 | 1991 Nov 23-24 | B | 6036 | 1 | EO875 |
| PKS2247 | 22 50 25.3 | 14 19 53 | $4.0 \times 10^{-14}$ | 4.8 | 700254 | 1991 Nov 26 | B | 7252 | 7 | EO800 |
| HR8905 | 23 25 22.1 | 23 24 13 | $3.0 \times 10^{-14}$ | 4.7 | 200322 | 1991 Jun 28-29 | B | 23424 | 3 | EO843 |

† For which optical identification is 89% complete.

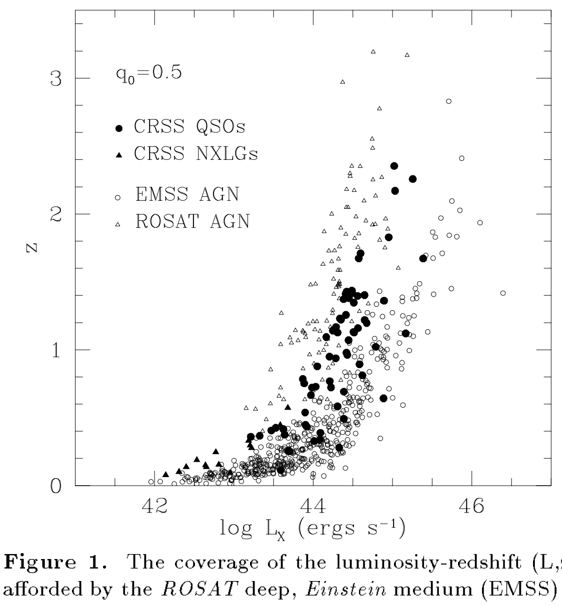


**Figure 1.** The coverage of the luminosity-redshift (L,z) plane afforded by the *ROSAT* deep, *Einstein* medium (EMSS) and the current surveys.

*ROSAT* PSPC fields used in the CRSS were selected to have high galactic latitude ($b^{II} > 30°$), exposure times greater than 5000 s and were available in the *ROSAT* archive prior to 1993 July. The fields were chosen to avoid bright or extended central sources which could otherwise affect the determination of the X-ray fluxes of the other sources identified in the field. To remove any remaining contribution from the central source, a central region 5 pixel in diameter on each field was excluded from any further analysis. The resulting sample included 20 fields with $14^{\rm h} < RA < 1^{\rm h}$ and $\delta > 0°$ (Table 1). In each field source detection was limited to within 15 arcmin of the field centre in order to maintain relatively high positional accuracy for the sources ($1\sigma$ error $\simeq 8$ arcsec) and to avoid obscuration by the rib support structure at larger off-axis angles.

The detection software used the IMAGES algorithm written by Dr Mike Irwin (now available as PISA in the STARLINK software collection). This software counts as a significant detection any source having four or more 15-arcsec pixels with counts $\gtrsim 1.5\ \sigma$ above the local background level. A limiting flux level of $S(0.5-2\,\mathrm{keV}) > 2 \times 10^{-14}\,\mathrm{erg\,s^{-1}\,cm^{-2}}$, significantly greater than the faintest flux detectable for point sources even on the fields with the shortest exposures, was then applied to the source list in order to ensure completeness for all but the most extended sources in this survey. We made no attempt to discriminate between extended and point sources identified by the algorithm. Counts were then determined for each remaining source using a 5 pixel (75 arcsec) diameter circle centered on the X-ray source. The net counts in the $0.5-2$ keV band ranged from 10 counts to 750 counts for detected sources in the CRSS with a median value of $\sim 50$ counts.

Background subtraction was made using a single level for the whole field (typically $\sim 2.3\times10^{-5}\,\mathrm{count\,s^{-1}\,pixel^{-1}}$), determined as the median level of the background within a circular region of 15-arcmin radius centered on the field center, after the removal of detected sources. The low background count rate results in the statistical error dominating the effects of vignetting so that no significant gradient is present. Based on a Poisson noise model, the error in the count determination is $\sim 15-20$ per cent at the flux limit of the survey. X-ray fluxes were determined from the net count rates of each source assuming $1\,\mathrm{count\,s^{-1}} = 1.2\times10^{-11}\,\mathrm{erg\,cm^{-2}\,s^{-1}}$. This value is appropriate for an X-ray energy spectral slope, $\alpha_E \sim 1.3$, typical of QSOs identified in this sample (see Paper IV), and also assuming that the Galactic absorption column has negligible effect for energies $> 0.5$ keV. These assumptions introduce an additional uncertainty ($\pm10$ per cent) in the reported X-ray fluxes due to the unknown spectral slope of each source.

Following the initial compilation of the catalogue, the X-ray source fluxes were subsequently revised using a much more sophisticated algorithm (see Paper IV). Full details of the X-ray flux measurement, including the source counts, background counts, hardness ratios, X-ray spectral slope and the associated errors for all the sources in the CRSS can be found in that paper.

However, for the purposes of this paper we prefer to report the original fluxes on which the initial selection of the catalogue was based. There is no significant systematic (i.e. luminosity-dependent) difference between the mean X-ray $0.5-2$ keV fluxes derived by the two methods, and the rms scatter ($\sim 20$ per cent) is consistent with the errors associated with the flux measurement for each method. We have verified that the use of the revised fluxes makes no significant difference to any of the results reported in this paper or in previous papers in this series (Papers I-II) where the original X-ray fluxes were used.

For 11 of the fields in this analysis, optical spectroscopic identification is 90 per cent complete to the X-ray flux limit. On the other fields, we subsequently imposed a brighter flux limit (listed in table 1) to ensure a similar level of spectroscopic completeness on these fields (see section 2.2).

A total of 123 serendipitous sources were identified in this survey. The pixel positions of each X-ray source were converted to RA, Dec using their offset from the central 'target' source in each PSPC field (usually a QSO) whose optical position was known to 1-arcsec accuracy.

## 2.2 Optical Candidates

APM measurements of Palomar Observatory Sky Survey (POSS) O and E plates (Irwin, Maddox & McMahon 1994) were used to generate a list of optical counterparts within 20 arcsec of each source. This radius represents 2.5 times the observed width of the X-ray to optical positional cross-correlation function (see Fig. 1(a) in Paper I). 112 of the 123 X-ray sources (91 per cent) had at least one optical counterpart within this range to the limit of the POSS plates ($O < 22$ mag, $E < 20$ mag). The typical error in the optical magnitudes determined from the POSS plates is $\pm0.2$ mag (Irwin et al. 1994). The mean $O-E$ colour of these counterparts is much bluer than the overall colour distribution (see Fig. 1(b) in Paper I), demonstrating that the counterparts are, as expected, dominated by QSOs ($O-E \sim 1$ mag, McMahon 1991). The X-ray source positions were subsequently revised to give a zero mean positional offset in each field between the X-ray and optical positions of sources with a blue ($O-E < 1.2$ mag) optical counterpart. This correction changed the nearest optical counterpart in 5 per cent of the total sample. The revised X-ray positions for all 123 sources are given in Table 2. The 0.5–2 keV fluxes for these sources and PSPC off-axis angle in arcminutes ($\theta$) are also given in this table, together with the optical positions, $O$ and $E$ magnitudes, and the optical-to-X-ray positional offset in arcseconds (O–X) for all the optical counterparts with spectroscopic identifications. The survey names were derived from the J2000 optical positions, X-ray positions were used when no optical identification was available.

## 2.3 Optical Spectroscopy

Low resolution ($3\mathrm{\AA\,pix^{-1}}$) spectroscopy was obtained for the optical counterparts with the ISIS double arm spectrograph at the William Herschel Telescope (WHT) on the nights of 1993 June 19–22. ISIS was operated with 158 lines/mm gratings in the blue and red arms (a dichroic filter was used to split the light at 5400Å), with the Tektronix and EEV CCDs as the detectors in the blue and red arms respectively.

Throughout the run the seeing was $\sim 1$ arcsec, and most of the observations were made with a 1.5 arcsec slit positioned at the parallactic angle. In these conditions, exposure times of 300–2400 sec were sufficient to yield an adequate signal-to-noise ratio ($\sim 10$) in the spectra of the vast majority of the optical candidates ($19 < O < 21$). With this set-up the overall instrumental resolution was 3Å. The spectra, fluxed with reference to a nearby standard star observed through the same spectrograph setup, are displayed in Fig. 2. Since a narrow slit was used, this is a relative flux scale; the absolute level is only accurate to $\sim \pm50$ per cent. The use of the dichroic results in a significantly decreased signal-to-noise ratio in the region around 5400Å, and occasionally gives rise to a spurious feature (usually a dip) around these wavelengths. In two cases (CRSS1415.1+1140 and CRSS2324.7+2315) an electronics fault resulted in no data from the red arm. However, the identification and redshift for both objects are secure from the blue arm data alone.

As far as possible, optical candidates in each PSPC field were observed in order of decreasing X-ray flux. This allowed us to incorporate any field for which we had not managed to observe all optical counterparts down to the original flux limit, $S(0.5-2\,\mathrm{keV}) > 2\times10^{-14}\,\mathrm{erg\,s^{-1}\,cm^{-2}}$, in the final survey, simply by imposing a brighter X-ray flux limit (i.e. the flux of the faintest X-ray source for which we observed the optical counterpart) for that field. This was the case for 9 PSPC fields. Based on the observing priority during the run (i.e. the candidates in the longer exposure PSPC fields were identified first) these 9 fields are mostly the shorter exposure PSPC fields in the survey.

## 2.4 Optical Identifications

As can be seen from Fig. 1(a) in Paper I, a significant number of optical images ($\sim 35$ per cent) identified within 20 arcsec will be chance coincidences, giving rise to multiple optical counterparts for some X-ray sources. For sources with more than one optical counterpart, optical spectroscopy was carried out in order of increasing separation between the X-ray position and optical counterpart until a plausible candidate (e.g. QSO, bright star, emission-line M star) was identified or we could be certain that we

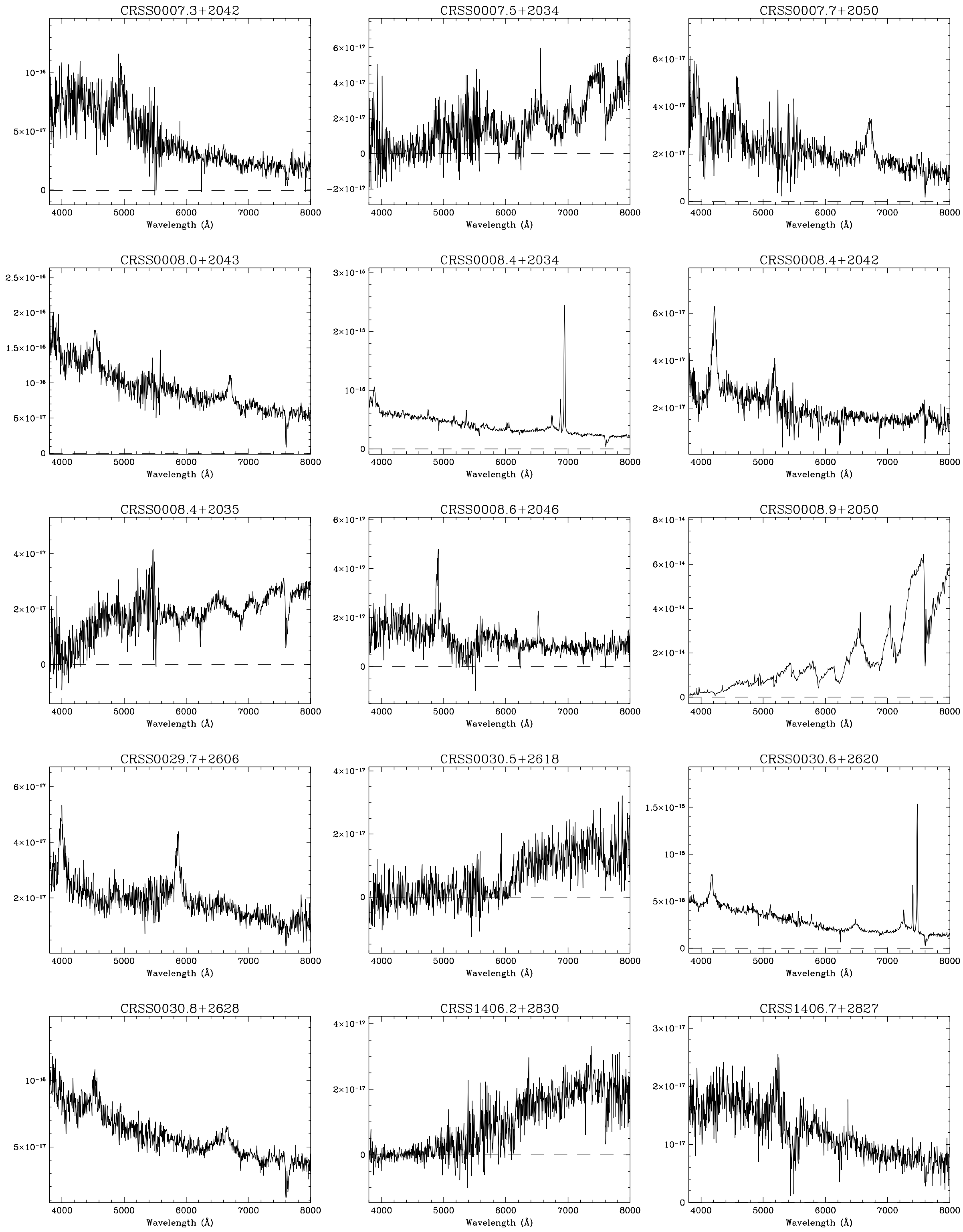


**Figure 2.** Optical spectra of the CRSS sources (excluding NLXG) extending from 3800–8000 Å at a resolution of $3\,\text{Å}\,\text{pix}^{-1}$ in units of $F_\lambda\,\text{erg}\,\text{cm}^{-2}\,\text{s}^{-1}\,\text{Å}^{-1}$.

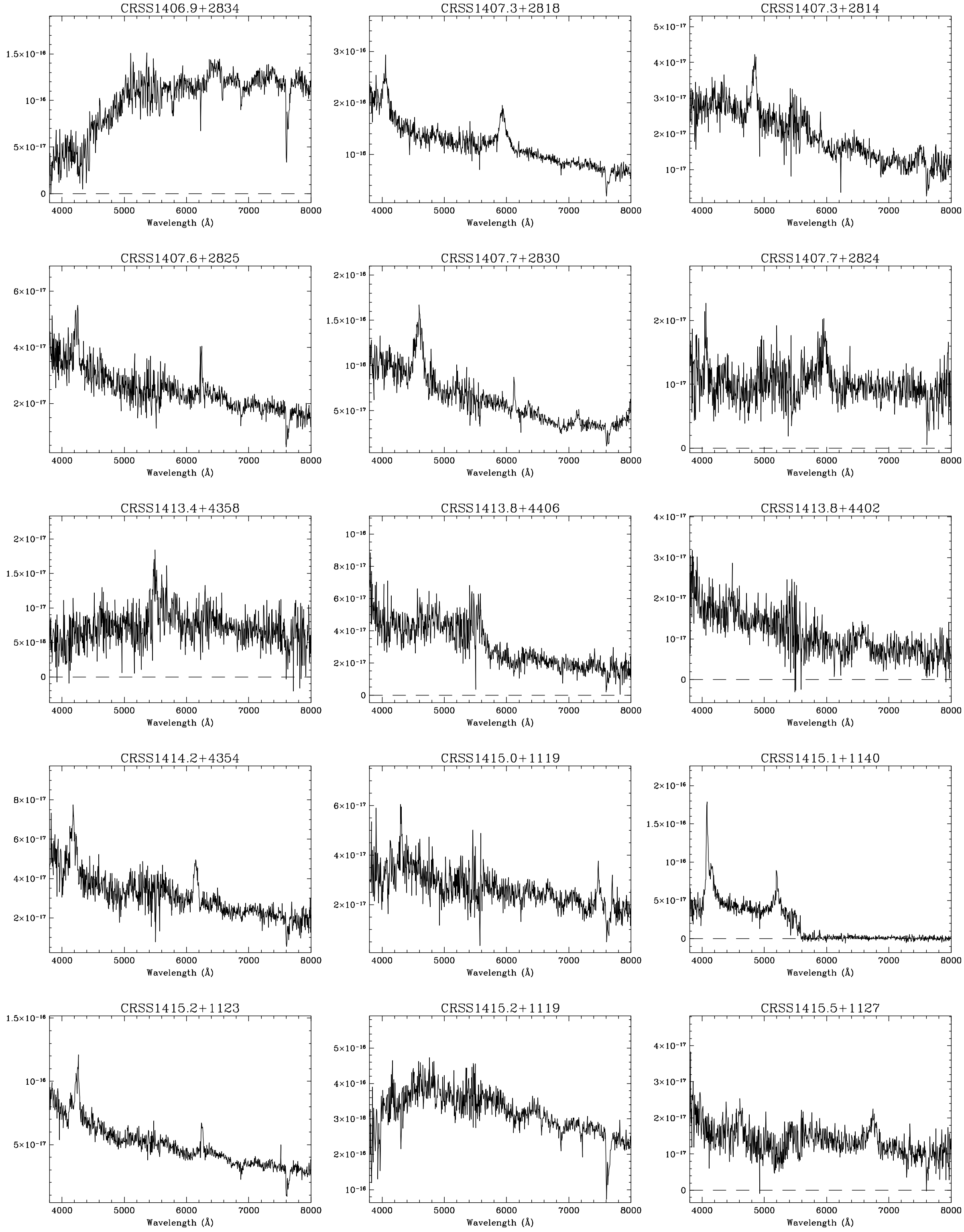


**Figure 2.** continued

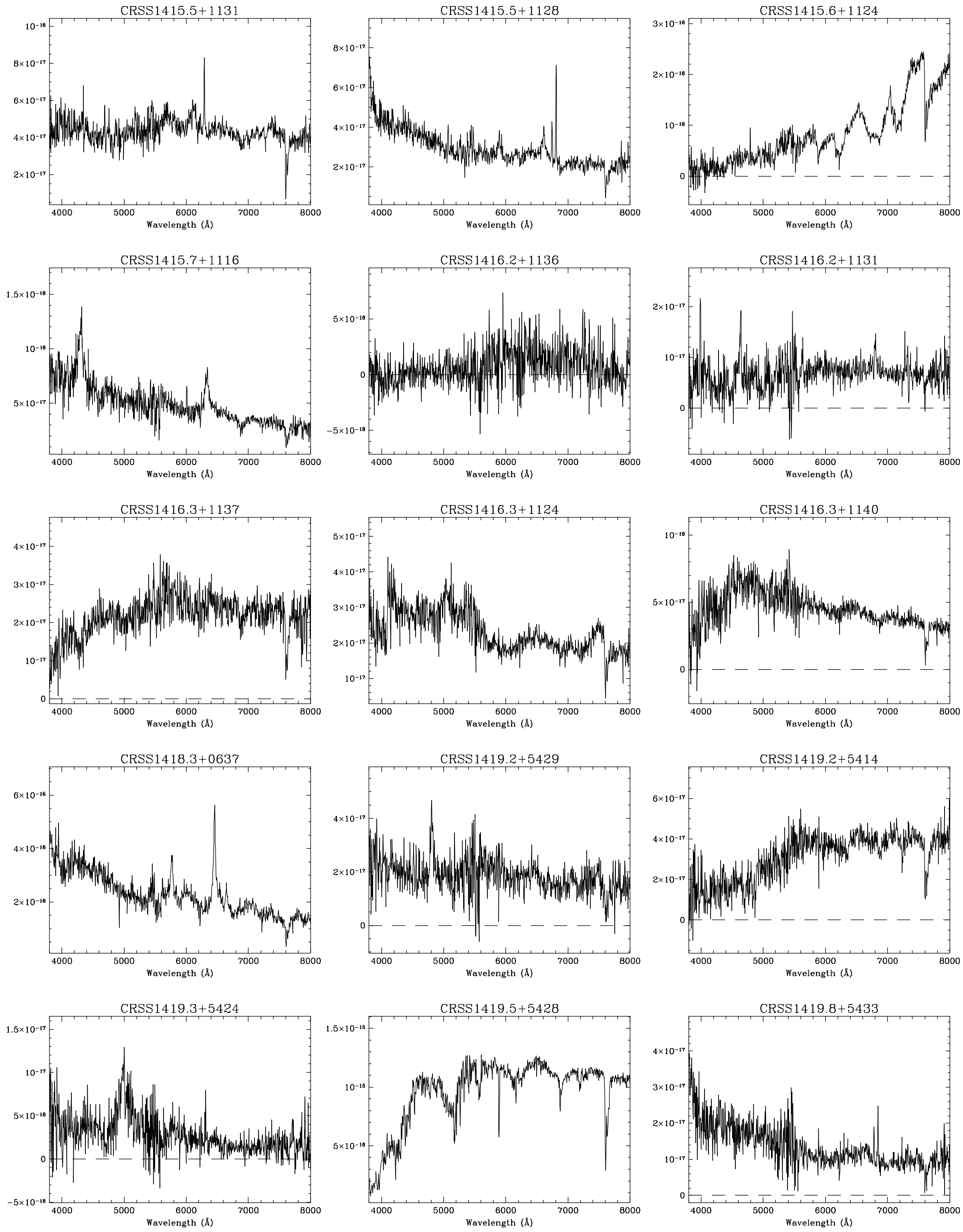


**Figure 2.** continued

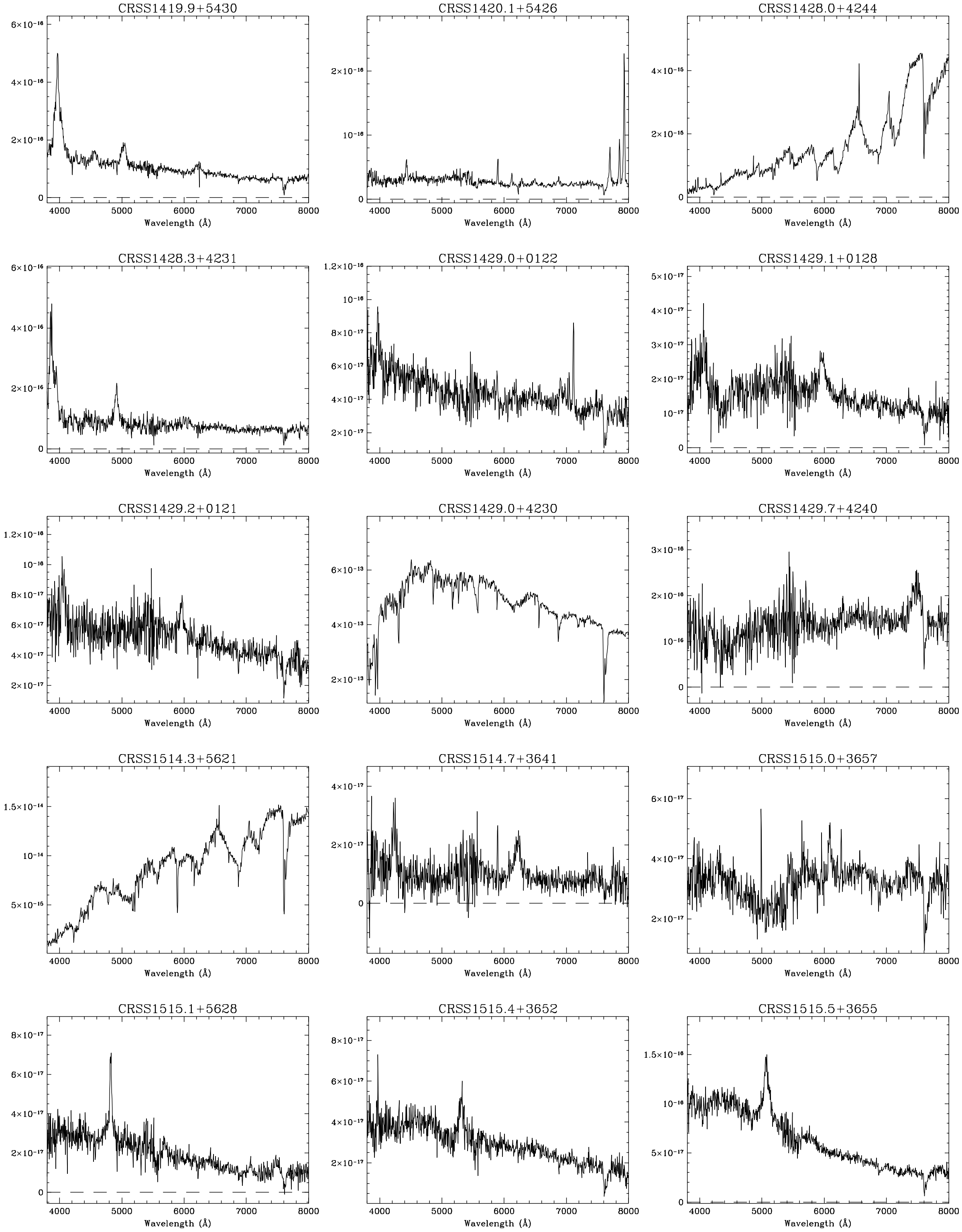


**Figure 2.** continued

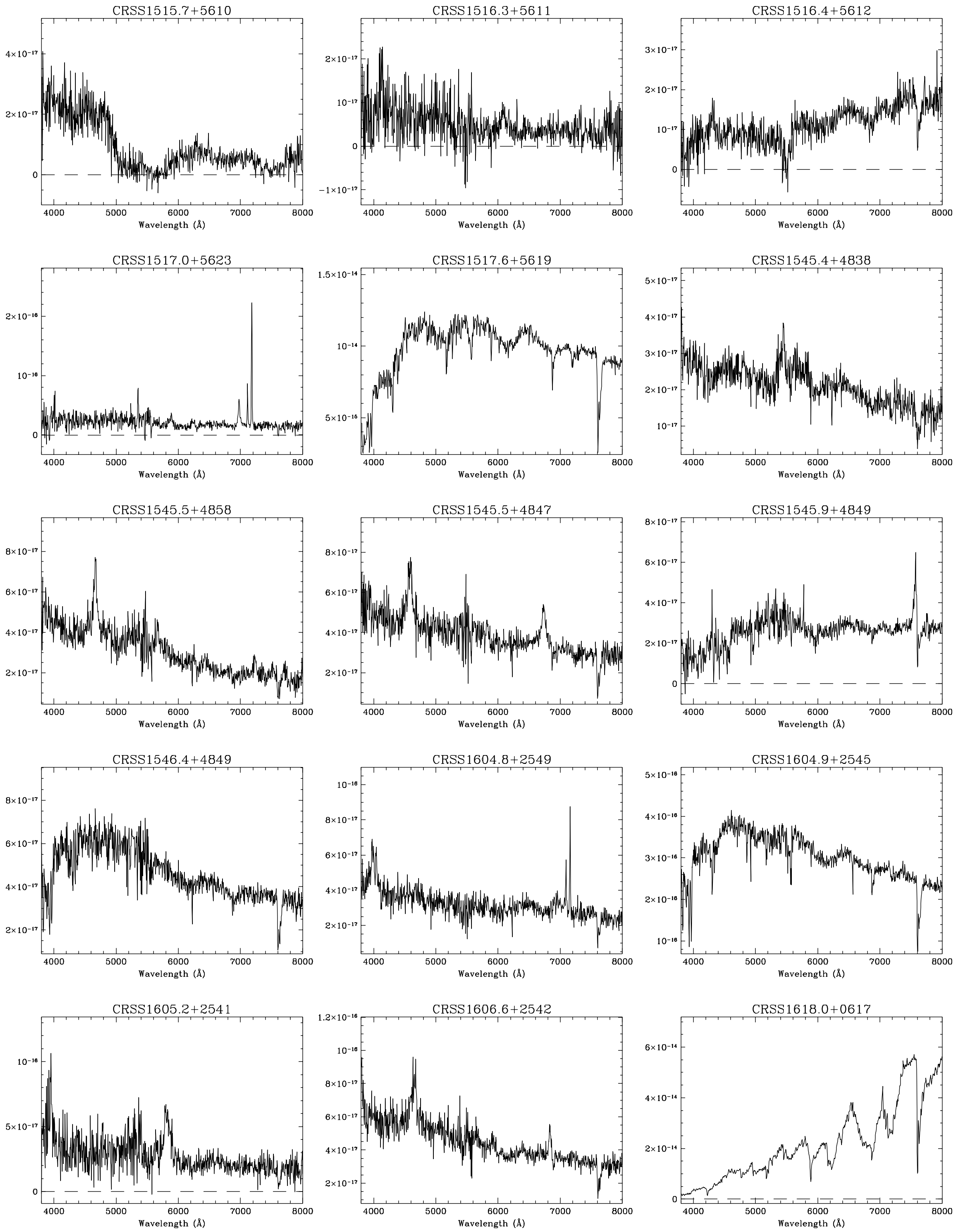


**Figure 2.** continued

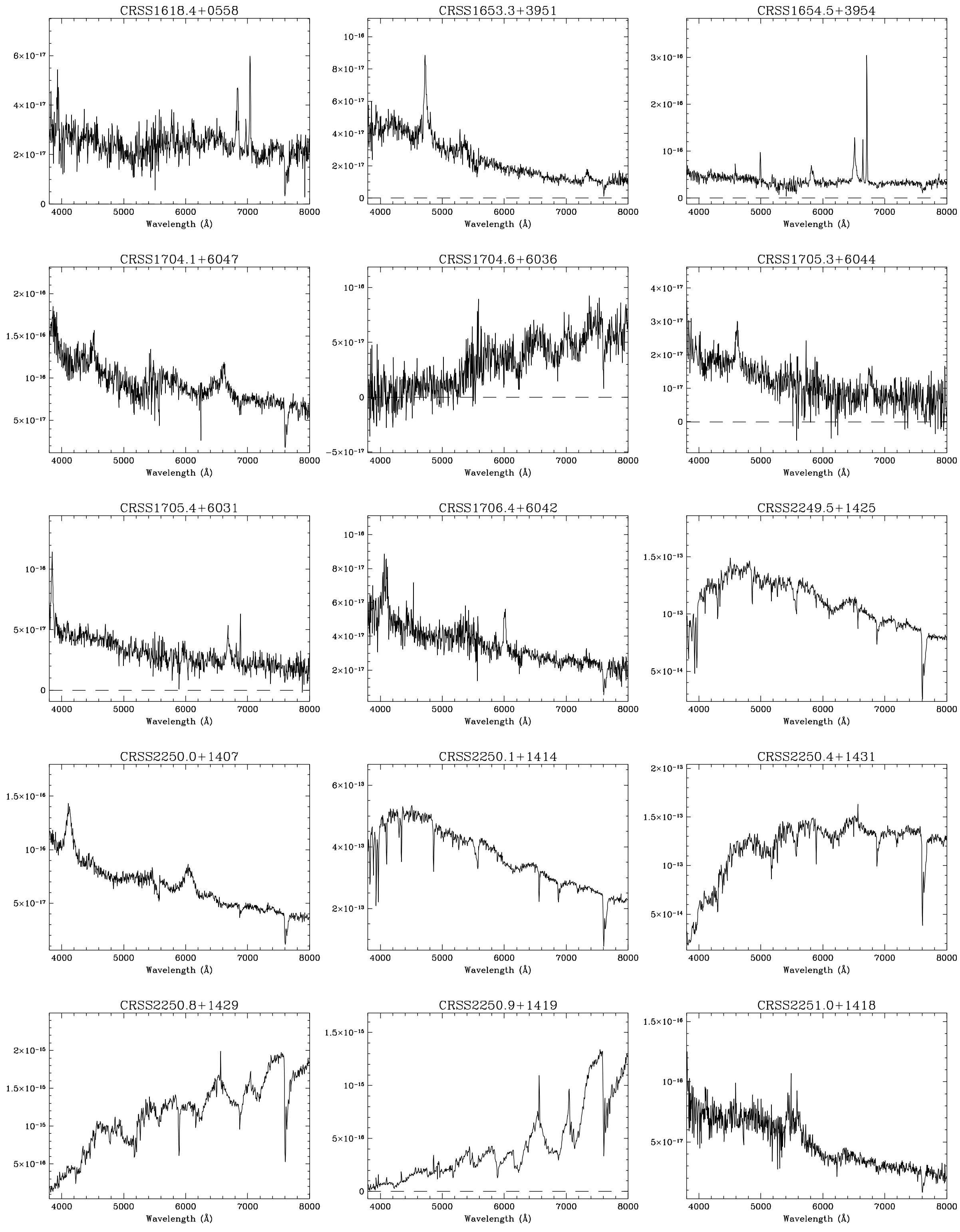


**Figure 2.** continued

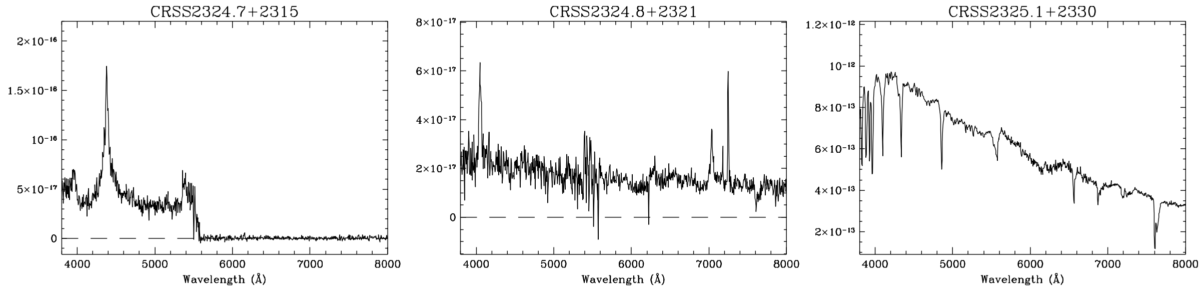


**Figure 2.** continued

**Table 3.** Summary of Identifications

| Identification | Number |
|---|---|
| QSO | 68 |
| NLXG | 12 |
| BL Lac | 2 |
| Early Type Galaxy | 2 |
| Galaxy Cluster | 2 |
| M Star | 11 |
| F/G Star | 11 |
| No optical counterpart | 11 |
| Optical counterpart not observed | 3 |
| Inconclusive optical spectrum | 1 |
| Total | 123 |

had the correct identification (i.e. two or more galaxies in a cluster). There was only one exception to this rule, CRSS1705.9+6046, where a blue stellar object lying 14 arcsec from the X-ray source position, was observed in preference to two fainter red stellar objects lying closer to the X-ray position. The identification of this object as a QSO confirmed that we had made the correct decision in this case. At the photographic plate limit, the *a priori* probability of identifying a QSO by chance in an error circle of 20arcsec radius is less than 0.01, based on a QSO surface density of 80 $\deg^{-2}$ at this magnitude (Boyle et al. 1991), and so we adopted this object as the 'true' optical counterpart of the X-ray source. Similarly, the surface density of bright ($R < 15$) stars at high galactic latitudes is only $\sim 100 \deg^{-2}$ (based on the star count models of Bahcall and Soniera 1980), resulting in a similarly low *a priori* probability of a chance coincidence.

In total, spectroscopic identifications for 118 optical candidates were obtained, including 4 objects with X-ray fluxes fainter than our final completeness limit and a further 4 objects (3 QSOs and 1 BL Lac) which had previously been identified. The observations resulted in an identification for 108 of the 123 X-ray sources in the CRSS. These optical identifications are listed in Table 2. We found that the closest optical counterpart was not the correct identification in only three cases (two QSOs and one NLXG) and a further three cases required observations of additional objects to confirm the identification. Each individual case of a multiple optical identification is discussed in the footnotes to Table 2. The optical spectra of all the true counterparts to the X-ray sources (excluding the NLXG, which were published in Paper I) identified on the basis of their WHT spectra are plotted in Fig. 2.

Table 3 summarises the source identification by object type. Of the 15 X-ray sources with no spectroscopic identification, two are bright stars ($O < 12$ mag) and we can assume these to be galactic stars with a high degree of confidence. A further 11 X-ray sources had no optical counterpart within 20 arcsec of the X-ray position on the POSS. Of the remaining two sources, the optical counterpart to the X-ray source CRSS1413.6+1156 had an inconclusive, low signal-to-noise spectrum and the counterparts to the X-ray source CRSS1405.6+2847 were not observed due to lack of time. A further object, CRSS1416.3+1137, was tentatively identified as a BL Lac based on the lack of any strong ($W_\lambda > 5$Å) emission or absorption lines in the optical spectrum. This equivalent width limit was also used by Stocke et al. (1991) to used identify candidate BL Lacs in the EMSS.

A KS test performed on the X-ray flux distribution of both the identified and unidentified sources (i.e. all those with no reliable spectroscopic identification, but excluding the two X-ray sources with bright stellar counterparts) revealed no significant differences between the flux distributions for the two samples at the 95 per cent confidence level. This implies that the incompleteness in the survey is independent of the X-ray flux level. Assuming the two bright stellar objects to be galactic stars, we obtain a 'spectroscopic' completeness of 89 per cent for the survey. To account for this incompleteness in the analysis below we have therefore multiplied the total area surveyed at each X-ray flux limit by 0.89 to yield effective survey areas. The area coverage of the survey can thus be derived straightforwardly from the field flux limits listed in Table 1. We note that in a few cases (up to 3) it is possible that we have identified a relatively faint F or G star which is not the true counterpart of the X-ray source. All such cases are discussed in the footnotes to Table 2. Removing these objects from the sample would reduce the completeness of the survey, but the 'loss' of these objects from the survey is likely to be compensated for by the detection of a similar number of galaxy groups or clusters detected in the 'blank' fields based on CCD imaging (see below).

## 2.5 CCD Imaging

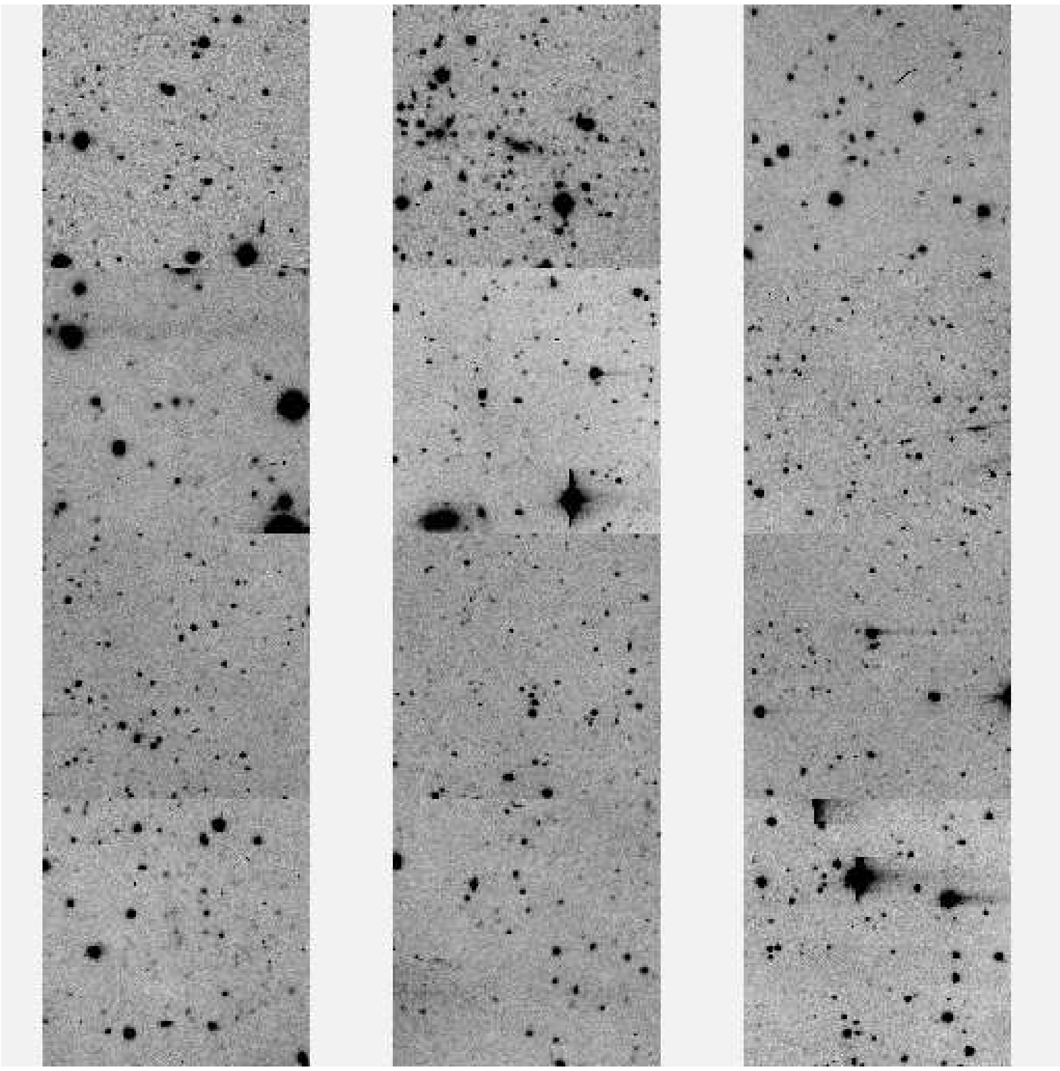

**Figure 3.** The CCD images for each of the POSS 'blank' fields and the $z = 0.52$ galaxy cluster field. In each frame a $3 \times 3$ arcmin region centred on the X-ray source position is shown. North is up and East is to the left. Top row (left to right): CRSS0029.1+2616, CRSS0030.5+2618 ($z = 0.52$ cluster) and CRSS1413.0+4406; second row: CRSS1413.9+4352, CRSS1415.3+1137 and CRSS1415.6+1127; third row: CRSS1415.9+1139, CRSS1416.0+1142 and CRSS1416.3+1129; bottom row: CRSS1429.1+4241, CRSS1516.8+5617 and CRSS1605.2+2602.

Intermediate-depth (600 s) $R$ band CCD images were obtained with the Isaac Newton Telescope for all of the fields with no optical counterpart on the POSS and one of the X-ray sources identified spectroscopically as a galaxy cluster (CRSS0030.5+2618). These observations were carried out as part of the service observation programme on 1994 May 12/13 and on 1995 October 18/19. Observations on 1994 May 12/13 were performed with the EEV CCD and observations on 1995 October 18/19 were carried out with the Tektronix CCD. Both CCDs have a pixel scale of 0.6 arcsec pix$^{-1}$. The seeing in both runs ranged from 1.5 to 2.5 arcsec (typically nearer the lower end of this range). Neither of the two nights was photometric. After bias-subtraction and flat-fielding, we carried out image detection on each CCD frame using the IMAGES routine (see section 2.1). Images with four or more connected pixels lying more than $2\sigma$ above the mean sky-background level were classified as real. Given the rather coarse pixel scale, we made no attempt to perform any classification of stars and galaxies; at the magnitude limit of the CCD frames ($R < 23$) the vast majority of the images ($> 90$ per cent) will be galaxies. In order to establish the significance of any group or cluster of galaxies seen at the position of the X-ray source on each CCD image, we compared the number of objects found within a 20-arcsec radius circle centred on the X-ray source position to the number expected based on the mean density of objects detected on that CCD frame. The results are presented in Table 4 and a mosaic of the CCD images based on $3 \times 3$-arcmin region surrounding each 'blank' field is plotted in Fig. 3.

Based on the $R$ galaxy counts published by Metcalfe et al. (1993), the mean image surface density on each field is consistent with an $R$ magnitude limit in the range ($22.5 < R < 23.25$). Out of the 11 'blank' fields, four (CRSS0029.1+2616, CRSS1413.0+4406, CRSS1416.3+1137 and CRSS1429.1+4241) exhibit a galaxy density twice that of the background and are likely to be galaxy groups or clusters. Although the numbers in any one field are small, the total numbers of images observed within the 20 arcsec radius on the four potential cluster fields is 24, compared to 9.9 expected based on the mean galaxy surface density in the field. This corresponds to a $4.5\sigma$ excess based on Poisson statistics. In contrast, we detect only 22 objects on the other 7 'blank' fields compared to 19.9 expected. Individual notes on the CCD images of the 'blank' fields are provided in Table 2.

The possible identification of a further 4 sources as groups/clusters brings the overall completeness of the CRSS to $\sim 92$ per cent. However, we prefer to retain the spectroscopic completeness ($\sim$ 89 per cent) factor in the analysis below, as the galaxy excess observed in these field has not positively been identified as being the true counterpart to the X-ray source. Indeed, we can not rule out the possibility that the counterpart to the X-ray source in any of these 'blank' fields is an object with a low optical-to-Xray flux ratio (e.g. an obscured AGN). However, the statisical excess of galaxies identified in these CCD frames argues that at least some of these X-ray sources are associated with galaxy groups or clusters.

We also observed the field of CRSS0030.5+2618 which was identified spectroscopically as a $z = 0.52$ galaxy cluster. The CCD image shows a very rich cluster (with a measured density 3 times that of the mean within the 20 arcsec radius). However, the brightness of the cluster galaxies imaged on the CCD is possibly indicative of a lower redshift than that derived from the spectroscopic observations and further observations are planned to investigate this discrepancy.

## 3 THE CATALOGUE

### 3.1 General Properties

The majority of the objects identified in the CRSS were QSOs (68, see Table 3), classified from the presence of one or more broad (FWHM $> 1000\,\mathrm{km\,s^{-1}}$) emission lines. A further 12 objects were identified as narrow-line X-ray luminous galaxies (NLXGs) and have been reported on extensively elsewhere (Papers I,II). Of the remaining 30 identifications, there are 2 early-type galaxies, 2 galaxy clusters ($z = 0.12$ and $z = 0.52$), 2 BL Lacs and 24 stars, comprising 11 M stars, 11 F/G stars and the two bright ($O < 12$ mag) stars which were not observed but are likely to be F/G stars. As described above, CCD observations of the fields of those X-ray sources without an optical counterpart on the POSS plate indicate up to a further 4 galaxy groups or clusters.

**Table 4.** CCD galaxy counts

| Source Name | Mean density $\mathrm{deg}^{-2}$ | Number in 20 arcsec circle Observed | Predicted |
|---|---|---|---|
| CRSS0029.1+2616 | 25795 | 5 | 2.3 |
| CRSS1413.0+4406 | 25048 | 6 | 2.4 |
| CRSS1413.9+4352 | 16713 | 3 | 1.6 |
| CRSS1415.3+1147 | 34150 | 1 | 3.3 |
| CRSS1415.6+1127 | 32115 | 6 | 3.1 |
| CRSS1415.9+1139 | 35296 | 1 | 3.4 |
| CRSS1416.0+1142 | 35396 | 4 | 3.4 |
| CRSS1416.3+1129 | 28281 | 8 | 2.7 |
| CRSS1429.1+4241 | 23730 | 5 | 2.3 |
| CRSS1516.8+5617 | 25563 | 3 | 2.6 |
| CRSS1605.2+2602 | 27230 | 4 | 2.6 |
| CRSS0030.5+2618† | 24621 | 8 | 2.5 |

† Spectroscopically identified as a $z = 0.52$ cluster.

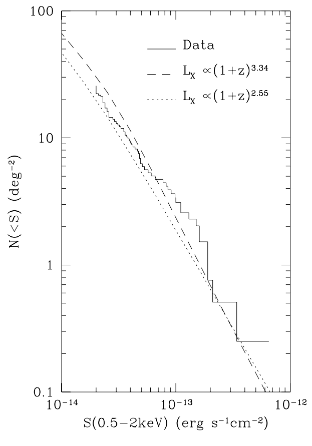


**Figure 4.** a) The cumulative number-flux relation for QSOs identified in the CRSS. The predictions of the QSO evolution models described in the text are also plotted.

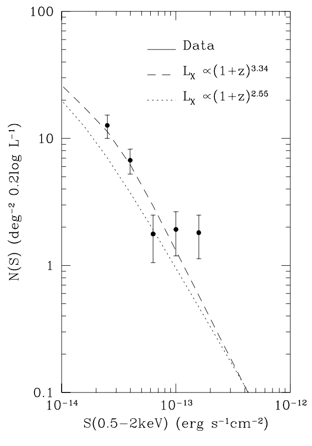


**Figure 4.** b) the same data plotted differentially.

### 3.2 QSOs

**Table 5.** QSO emission line measurements

| Name | $z$ | Ly$\alpha$/NV | | CIV | | CIII] | | MgII | | H$\beta$ | |
|---|---|---|---|---|---|---|---|---|---|---|---|
| | | $W_{\lambda_0}$ | $\Delta v$ | $W_{\lambda_0}$ | $\Delta v$ | $W_{\lambda_0}$ | $\Delta v$ | $W_{\lambda_0}$ | $\Delta v$ | $W_{\lambda_0}$ | $\Delta v$ |
| 0007.3+2042 | 0.769 | | | | | | | 47 | 7.7 | | |
| 0007.7+2050 | 1.396 | | | $75^a$ | 6.0 | $23^a$ | 4.8 | 44 | 5.2 | | |
| 0008.0+2043 | 1.381 | | | 37 | 12.0 | 13 | 5.1 | 12 | 2.9 | | |
| 0008.4+2034 | 0.389 | | | | | | | $39^a$ | 4.9 | $19^a$ | 5.3 |
| 0008.4+2042 | 1.710 | | | 35 | 5.8 | 11 | 3.0 | 25 | 6.0 | | |
| 0008.6+2046 | 0.752 | | | | | | | 57 | 2.9 | 65 | 2.2 |
| 0029.7+2606 | 1.094 | | | | | 23 | 5.3 | 32 | 4.0 | | |
| 0030.6+2620 | 0.493 | | | | | | | 30 | 5.4 | 74 | $8.1^b$ |
| 0030.8+2628 | 1.372 | | | $17^a$ | 3.9 | $14^a$ | 6.9 | 34 | 12.2 | | |
| 1406.7+2827 | 0.878 | | | | | | | 25 | 6.6 | | |
| 1407.3+2818 | 1.121 | | | | | $15^a$ | 4.4 | $40^a$ | 5.4 | | |
| 1407.3+2814 | 0.728 | | | | | | | 33 | 5.6 | 36 | 2.6 |
| 1407.6+2825 | 1.222 | | | | | 14 | 4.8 | $8^a$ | 1.7 | | |
| 1407.7+2830 | 0.642 | | | | | | | $57^a$ | 8.2 | 65 | 8.0 |
| 1407.7+2824 | 1.127 | | | | | 22 | 4.4 | 17 | 3.2 | | |
| 1413.4+4358 | 0.950 | | | | | | | $74^a$ | | | |
| 1413.8+4406 | 0.978 | | | | | 17 | 4.3 | $35^a$ | | | |
| 1413.8+4402 | 1.347 | | | $52^a$ | 6.9 | $12^a$ | | $59^a$ | 9 | | |
| 1414.2+4354 | 1.197 | | | | | 35 | 8.3 | $21^a$ | 3.2 | | |
| 1415.0+1119 | 0.538 | | | | | | | 12 | 2.9 | $40^a$ | 1.8 |
| 1415.1+1140 | 2.353 | $55^a$ | 2.7 | 8 | 1.6 | | | | | | |
| 1415.2+1123 | 1.230 | | | 18 | 5.5 | 7 | 1.5 | | | | |
| 1415.5+1127 | 1.412 | | | 24 | 5.5 | 9 | 3.5 | 20 | 4.5 | | |
| 1415.5+1131 | 0.257 | | | | | | | | | 14 | 3.8 |
| 1415.5+1128 | 0.360 | | | | | | | 15 | 3.9 | 20 | 2.9 |
| 1415.7+1140 | 1.257 | | | | | 20 | 5.3 | 17 | 2.9 | | |
| 1416.2+1131 | 1.429 | | | | | 21 | 2.2 | 7 | 2.0 | | |
| 1416.3+1124 | 1.673 | | | $12^a$ | | 12 | 7.7 | 32 | 9.3 | | |
| 1418.3+0637 | 0.329 | | | | | | | | | $66^a$ | 1.7 |
| 1418.4+0558 | 0.406 | | | | | | | 15 | 2.4 | 29 | 1.6 |
| 1419.2+5429 | 0.722 | | | | | | | 31 | 2.9 | 54 | 3.0 |
| 1419.3+5424 | $0.785^d$ | | | | | | | $135^a$ | 10.0 | | |
| 1419.8+5433 | 0.367 | | | | | | | 18 | 4.9 | 23 | 5.7 |
| 1419.9+5430 | 2.257 | $53^a$ | 4.9 | 14 | 4.8 | 8 | 4.6 | | | | |
| 1420.1+5426 | 0.583 | | | | | | | 13 | 1.5 | 40 | 1.1 |
| 1428.3+4231 | 2.171 | $67^a$ | 4.2 | $21^a$ | 3.0 | $15^a$ | | | | | |
| 1429.0+0122 | 0.416 | | | | | | | 20 | 4.5 | 32 | 6.6 |
| 1429.1+0128 | 1.131 | | | | | | | 19 | 4.2 | | |
| 1429.2+0121 | 1.127 | | | | | 13 | 4.5 | 11 | 3.2 | | |
| 1429.7+4240 | 1.672 | | | | | | | 33 | 6.3 | | |
| 1514.7+3641 | 1.219 | | | | | 37 | 4.3 | 44 | 4.6 | | |
| 1515.0+3657 | 0.253 | | | | | | | | | $88^c$ | $2.2^c$ |
| 1515.1+5628 | 0.723 | | | | | | | 23 | 2.1 | 23 | 1.2 |
| 1515.4+3652 | 0.893 | | | | | $22^a$ | 1.6 | 26 | 4.5 | | |
| 1515.5+3655 | 0.812 | | | | | | | $40^a$ | 5.3 | | |
| 1515.7+5610 | 0.296 | | | | | | | | | $59^c$ | $1.7^c$ |
| 1516.3+5611 | 1.168 | | | | | 21 | 3.3 | 38 | 4.5 | | |
| 1517.0+5623 | 0.434 | | | | | | | 28 | 2.4 | 56 | 1.5 |
| 1545.4+4838 | 0.937 | | | | | $20^a$ | | $19^a$ | | | |
| 1545.5+4858 | 0.666 | | | | | | | 28 | 3.9 | 29 | 2.1 |
| 1545.5+4847 | 1.403 | | | | | 25 | 6.5 | 11 | 3.8 | | |
| 1545.9+4849 | 0.154 | | | | | | | | | | |
| 1604.8+2549 | 0.426 | | | | | | | 24 | 7.3 | 33 | 7.4 |
| 1605.2+2541 | 1.071 | | | | | $48^a$ | | 61 | 5.5 | | |
| 1606.6+2542 | 1.436 | | | 28 | 5.3 | 13 | 5.1 | 7 | 1.7 | | |
| 1653.3+3951 | 0.692 | | | | | | | $50^a$ | 2.8 | $46^a$ | 3.2 |
| 1654.5+3954 | 0.340 | | | | | | | 44 | 2.2 | 61 | 1.0 |
| 1704.1+6031 | 1.362 | | | 25 | 3.9 | 5 | 2.9 | 8 | 3.3 | | |
| 1705.4+6031 | 0.375 | | | | | | | 20 | 2.5 | 40 | 2.6 |

**Table 5.** contd.

| Name | $z$ | Ly$\alpha$/NV | | CIV | | CIII] | | MgII | | H$\beta$ | |
|---|---|---|---|---|---|---|---|---|---|---|---|
| | | $W_{\lambda_0}$ | $\Delta v$ | $W_{\lambda_0}$ | $\Delta v$ | $W_{\lambda_0}$ | $\Delta v$ | $W_{\lambda_0}$ | $\Delta v$ | $W_{\lambda_0}$ | $\Delta v$ |
| 1705.3+6044 | 1.416 | | | 37 | 4.4 | 12 | 3.3 | 22[a] | | | |
| 1706.4+6042 | 1.142 | | | | | 22 | 6.6 | 14 | 2.1 | | |
| 2250.0+1407 | 1.159 | | | | | 19 | 7.4 | 28 | 8.2 | | |
| 2251.0+1418 | 0.962 | | | | | 18 | 5.4 | 39 | 12 | | |
| 2324.7+2315 | 1.828 | | | 51 | 3.2 | | | | | | |
| 2324.8+2321 | 0.447 | | | | | | | 40 | 2.7 | 33 | 1.4 |

Rest equivalent width ($W_{\lambda_0}$) is given in Å.
Rest FWHM ($\Delta v$) is given in units of $10^3\,\mathrm{km\,s^{-1}}$

[a] Gaussian fit inappropriate/impossible for this line.
[b] H$\beta$ broad component only.
[c] H$\alpha$ measurements.
[d] In the absence of CIV, the single line is identified as MgII. Its high equivalent width suggests an ID of Ly$\alpha$ with $z = 3.108$, although the proximity of the emission line to the dichroic cut-off could also be a factor.

### *3.2.1 Space Density*

The number-flux, $\log N - \log S$, and number-redshift, $n(z)$, relations for the 68 QSOs identified in this survey are plotted in Figs. 4a, b and 5. We also plot in these figures the predicted $\log N - \log S$ and $n(z)$ relations based on cosmological evolution of the X-ray (0.3 − 3.5 keV) luminosity function derived from fits to the *Einstein* Medium Sensitivity Survey (EMSS, Maccacaro et al. 1991) and the deep *ROSAT* survey (Boyle et al. 1994). As demonstrated by Maccacaro et al. (1991) the EMSS yields a slow rate of luminosity evolution ($L_X \propto (1+z)^{k_L}$, $k_L = 2.55 \pm 0.1$), whereas much faster rates are derived are derived from the deep *ROSAT* survey ($k_L = 3.34 \pm 0.1$, Boyle et al. 1994) when a cut-off in the evolution at $z_{\max} = 1.79$ is included. We have used the fits provided by Boyle et al. (1993, model J) and Boyle et al. (1994, model S) for the EMSS and deep *ROSAT* samples respectively. Both models assume $q_0 = 0$, $H_0 = 50\,\mathrm{km\,s^{-1}\,Mpc^{-1}}$ and $\alpha_E = 1$ in order to maintain consistency with the values adopted previously for these parameters by Maccacaro et al. (1991). This value of $\alpha_E$ is different to mean value obtained for the CRSS sample ($\alpha_E = 1.3$, Paper IV). However, an increase in the adopted value for $\alpha_E$ would simply translates to an equal increase in the derived value of $k_L$ in these models. The predicted $n(z)$ relations for all models have been normalized to the total number of QSOs observed in the CRSS. Note that NLXGs are not included in either relation.

The observed $\log N - \log S$ relations agrees more closely with the predictions of the model derived from the *ROSAT* deep survey (Boyle et al. 1994), confirming the faster rate of X-ray luminosity evolution ($k_L = 3.34 \pm 0.1$, $z_{\max} = 1.79$) for QSOs derived in the *ROSAT* energy range. This is apparent in Fig. 4 where the slower rate of X-ray evolution ($k_L = 2.55 \pm 0.1$) in the *Einstein* data (EMSS, Maccacaro et al. 1991) predicts a lower $\log N - \log S$ relation leading to an expected number of QSOs in the CRSS of 41 compared to the 68 observed. The *ROSAT* deep survey model predicts 62. Based on purely Poission statistics, the EMSS-based model can therefore be ruled out at the 3.3$\sigma$ level.

In Fig. 5, the EMSS slower rate of evolution results in a predicted $n(z)$ for the CRSS sample which is more heavily weighted towards low redshifts than is observed. Formal comparison of the observed and predicted $n(z)$ distributions using a one-dimensional KS test over the range $0 < z < 3$ concludes that the EMSS prediction is different at greater than the 99 per cent confidence level ($P_{KS} = 0.003$) whereas the *ROSAT* deep survey prediction can not be rejected even at the 95 confidence level ($P_{KS} = 0.082$).

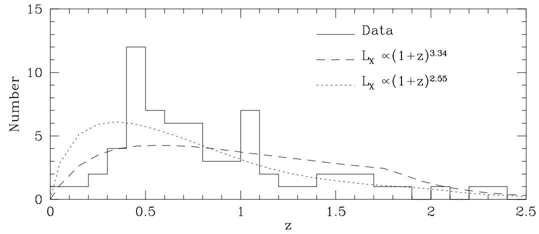


**Figure 5.** The integral number-redshift relation for QSOs identified in the CRSS. The predictions of the two QSO evolution models described in the text are also plotted.

Recent analyses of QSOs identified in the RIXOS (Page et al. 1996) and UK Deep Surveys (Jones et al. 1996) have yielded evolutionary rates $k_L = 2.9$, intermediate between the rates discussed here. Both these models also incorporate a redshift cut-off ($1.63 < z_{\max} < 1.82$), consistent with that derived by Boyle et al. (1994). However, we note that both these analyses include the EMSS sample with the RIXOS or UK Deep sample in the determination of the evolution. This is in contrast to the models discussed above which are based on the analysis of the EMSS and *ROSAT* Deep surveys seperately.

Note that Boyle et al. (1994) also derive an intermediate evolutionary rate ($k_L = 3.0 \pm 0.1$, $z_{\max} = 1.89$) when the EMSS is included with the *ROSAT* sample in the overall fit. Similarly, the best-fit evolution model to the radio-quiet QSOs in the combined EMSS and CRSS surveys has $k_L = 2.7 \pm 0.1$, with no redshift cut-off (Paper III). This is in good agreement with the fit to the combined RIXOS and EMSS survey derived by Page et al. (1996) ($k_L = 2.66$) for a similar evolution model with no redshift cut-off. It thus appears to be a general feature of these fits that the inclusion of the *Einstein*-selected EMSS slows the evolutionary rate that would otherwise be derived from samples of QSOs based on *ROSAT* surveys alone. It will be interesting to see whether surveys such as the RIXOS (Page et al. 1996) or *ROSAT* Deep survey (Jones et al. 1996) confirm this behaviour.

### *3.2.2 Emission Line Properties*

The broad emission lines for all the QSOs newly discovered in this survey were measured using IRAF. The rest frame equivalent widths and full width at half maximum (FWHM) are given in Table 5. The redshift is repeated for convenience. Given the generally low quality of the data, no attempt was made to deblend the dominant lines from the weaker features with which they are blended, nor was any deblending of the broad and narrow components of H$\beta$ attempted unless the separation was clear (labelled in Table 5). A local, linear continuum was used in combination with a Gaussian profile fit where appropriate, otherwise the data were measured directly (also indicated in Table 5). The accuracy of the line measurements is estimated at $\pm 30$ per cent. The distributions (mean and dispersion assuming a Gaussian distribution) of equivalent widths and FWHM are given in Table 6. The equivalent widths are similar to those from surveys including those in other wavebands. The numbers for Parkes radio-selected, flat radio spectrum QSOs (Wilkes et al. 1983, Wilkes 1986, Wilkes 1982) are shown for illustration.

We note a few interesting discrepancies with recent datasets. Although the equivalent width of H$\beta$ agrees well with that of the radio-selected QSOs, its value is approximately half that of the optically selected PG sample (96Å$\pm$ 37Å, Boroson & Green 1992). This latter dataset has high signal-to-noise (S/N) spectra and a detailed deblending of H$\beta$ from surrounding weak FeII features was performed. It is possible that the low S/N of the optical spectra of both the radio- and X-ray selected samples results in the blended FeII emission systematically raising the apparent continuum level around H$\beta$ and lowering the apparent line strength. Clearly, higher S/N optical data are necessary to investigate this further.

It has been reported that radio-loud QSOs have narrower UV lines than radio-quiet QSOs (Francis, Hooper & Impey 1993, Brotherton et al. 1994, Baldwin, Wampler & Gaskell 1989), a difference which has been interpreted in terms of differing structure and line ratios in the emitting region. This difference is most notable for the CIII]$\lambda$1909 line due to its blending with AlIII$\lambda$1858. In the current X-ray-selected, predominantly radio-quiet (Ciliegi et al. 1995) sample, the FWHM of the CIII] blend agrees with that of the radio-loud (5000-6000 kms$^{-1}$) rather than the radio-quiet (7000-9000 kms$^{-1}$) QSOs in these earlier papers. This implies that X-ray emission is a factor in determining the UV emission line widths such that X-ray selection results in a systematically different (narrower emission line) subset of the radio-quiet QSO population than optical selection. The correlation between optical-to-X-ray flux ratio and the X-ray spectral index present in the optically-selected sample of Laor et al. (1996) predicts the opposite effect since in their sample the X-ray loud objects have broader lines. Clearly, confirmation and a definitive interpretation of these results must await a detailed investigation using higher quality optical spectra.

**Table 6.** Distribution of Emission Line Measurements

| Line | $W_{\lambda_0}$ (Å) Mean | $\sigma$ | No. | FWHM/$10^3$ km s$^{-1}$ Mean | $\sigma$ | No. |
|---|---|---|---|---|---|---|
| CIV | 30(32) | 18 | 15 | 5.1(5.0) | 2.4 | 14 |
| CIII] | 18(17) | 9 | 32 | 4.8(5.8) | 1.8 | 28 |
| MgII | 29(27) | 16 | 53 | 4.7(4.3) | 2.6 | 50 |
| H$\beta$ | 41(47) | 18 | 21 | 3.4(4.8) | 2.4 | 21 |

The numbers in brackets are for Parkes flat-spectrum radio-selected QSOs.

The strongest correlation reported by Laor et al. (1994, 1996) is an inverse relation between the FWHM(H$\beta$) and the soft X-ray slope for their sample of low-redshift PG QSOs. In addition, Boller, Brandt & Fink (1996) report a strong tendency for QSOs with narrower lines to have much steeper (softer) X-ray spectra. We tested for such a relation in our sample using the X-ray slopes reported in Paper IV, but found none. We also found no relation between the X-ray slope and the FWHM for CIV$\lambda$1549, CIII]$\lambda$1909, or MgII$\lambda$2798 (see Figure 6). Notably, our sample was selected in the *ROSAT* hard band ($0.5-2$ keV) and so is biased against the unusually soft sources reported by Boller et al. (1996) and includes a significantly smaller range of X-ray slopes than the optically-selected sample ($\Delta\alpha_{\rm E}\sim 1$ cf. $\Delta\alpha_{\rm E}\sim 2$ of Laor et al. 1996). It seems likely that the different selection criteria combined with the smaller distribution of X-ray slopes combine to mask any correlation in our sample.

## 4 CONCLUSIONS

Here we summarise the conclusions of all five papers in this series. Our spectroscopic survey of 123 sources detected in a medium-depth *ROSAT* survey ($S(0.5-2\,{\rm keV}) > 2\times10^{-14}$ erg s$^{-1}$ cm$^{-2}$) has yielded new identifications for 108 objects; including 68 QSOs, 12 narrow emisson-line X-ray galaxies, 22 stars, 2 BL Lac objects, 2 galaxies and 2 clusters. In addition, two X-ray sources are coincident with bright stars and deep CCD imaging reveals tentative evidence for faint galaxy groups/clusters at the positions of a further 4 sources. In total, a possible identification exists for up to 92 per cent of the sources in the CRSS. In this paper we have shown that the number-flux and number-redshift relations for QSOs identified in this survey are consistent with the fast rate of cosmological luminosity evolution previously derived from deep *ROSAT* surveys ($L_X \propto (1+z)^{3.34\pm0.1}$). The emission-line equivalent width distribution for the X-ray QSOs identified in this survey is similar to those determined from surveys at other wavelengths. The line widths, specifically that of the CIII] blend, are more similar to radio-loud than optically-selected, radio-quiet objects implying that X-ray selection affects the emission line properties of the sample. We do not confirm an inverse correlation between the emission line width and the X-ray spectral slope, which is probably due to the different selection and properties of the comparative samples.

The NLXGs in both the current and EMSS samples, discussed in Papers I & II, comprise a rougly equal mix of AGN and starburst galaxies as distinguished by their optical

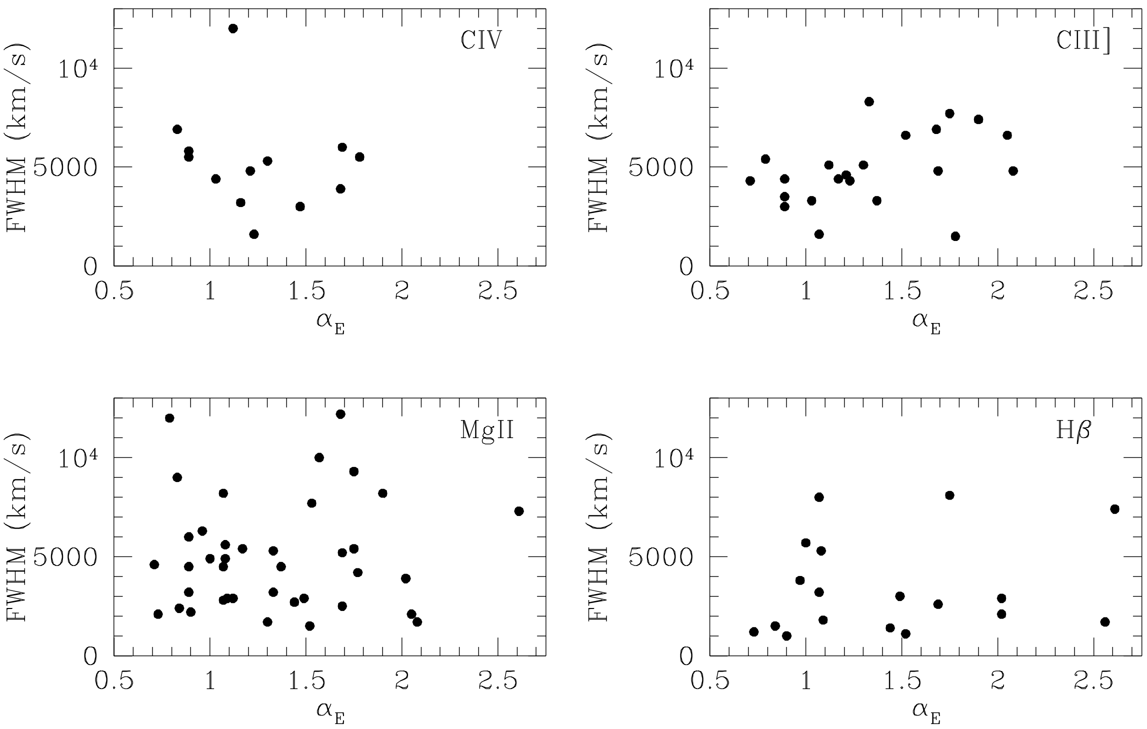


**Figure 5.** Widths of the prominant emission line blends as a function of the ROSAT X-ray spectral slope.

emission line ratios. Their X-ray evolution and X-ray spectral properties (see also Paper IV) are indistinguishable from one another and from those of QSOs. We estimate that the two classes contribute approximately equally to the X-ray background at a level of $\sim 10$ per cent (Paper I,II).

The X-ray luminosity function for radio-loud and radio-quiet QSOs in the combined CRSS and EMSS sample shows that, while the luminosity evolution is similar in the two classes, the shape of the de-evolved luminosity function is different (Paper III). This difference can be explained in terms of the additional, beamed, radio-linked X-ray component, commonly believed to be present in radio-loud QSOs (e.g. Shastri et al. 1993, Wilkes & Elvis 1987, Zamorani et al. 1981).

A detailed analysis of the X-ray spectral properties of QSOs and NLXGs over the full $0.1 - 2.4$ keV energy range of the *ROSAT* PSPC (Paper IV) demonstrates that a single power law slope with Galactic absorbing column density yields a good fit for the majority of sources. The mean slope for the QSOs is 1.3 with a dispersion of 0.5 and no redshift dependence. The most probable explanation of this latter result is that these QSOs exhibit a single power-law X-ray spectrum from $0.1 - 7.3$ keV with no change in slope. In contrast, the CRSS NLXGs do show evidence for a decrease in their spectral slope with redshift.

## ACKNOWLEDGEMENTS

BJB acknowledges the support and hospitality of the Smithsonian Astrophysical Observatory. The X-ray data was obtained from the Leicester and Goddard *ROSAT* archives. This work was partially supported by NASA grants NAGW-2201 (LTSA) and NAG5-3066 (ADP) and NASA contracts NAS5-30934 (RSDC) and NAS8-39073 (ASC). The optical spectra were obtained at the William Herschel Telescope at the Observatory of the Roque de los Muchachos operated by the Royal Greenwich Observatory.

## REFERENCES

Bahcall J. N. Soniera R., 1980, ApJS, 44, 73
Baldwin, J.A., Wampler, E.J. & Gaskell, C.M. 1989 ApJ 338, 630
Boller, T. Brandt, W.N., Fink, H.H. 1996, A&A, 305, 53
Boroson, T.A. & Green, R.F. 1992 ApJS 80, 109
Boyle B.J., Jones L.R., Shanks T. 1991, MNRAS, 251, 482
Boyle B.J., Shanks T., Georgantopoulos I.G., Stewart G.C., Griffiths R.E., 1994, MNRAS, 271, 639
Boyle B.J., McMahon R.G., Wilkes B.J., Elvis M. 1995a MNRAS 272, 462 (Paper I)
Boyle B.J., McMahon R.G., Wilkes B.J., Elvis M. 1995b MNRAS 276, 315 (Paper II)
Branduardi-Raymont G., et al., 1994, MNRAS, 270, 497
Brotherton, M.S., Wills, B.J., Steidel, C.C. & Sargent, W.L.W. 1994 ApJ 423, 131
Ciliegi P., Elvis M., Wilkes B.J., Boyle B.J., McMahon R.G., Maccacaro T., 1995, MNRAS, 277, 1463 (Paper III)
Ciliegi P., Elvis M., Wilkes B.J., Boyle B.J., McMahon R.G., Maccacaro T., 1996, MNRAS, in press, (Paper IV)
Crampton D., Cowley A.P., Hartwick F.D.A., 1987, Ap.J., 268, 565
Francis, P.J., Hooper, E.J. & Impey, C.D. 1993 AJ, 106, 417
Gioia I.M., Maccacaro T., Schild R. E., Wolter A., Stocke J.T., Morris S.L., Henry J.P., 1990, ApJS, 72, 567
Irwin, M.J., Maddox, S.J., McMahon, R.G. 1994 Spectrum, 2 14
Jones L.R., et al., 1996, in Zimmermann H.U., Trümper J.E., Yorke H. eds, MPE Report 263, Röntgenstrahlung from the

Universe, Max-Planck-Institute für Extraterrestrische Physik, Garching, p457
Hasinger G., Burg R., Giacconi R., Hartner G., Schmidt M., Trümper J., Zamorani G., 1993, A&A, 275, 1
Maccacaro T., Dela Ceca R., Gioia I.M., Morris S.L., Stocke J.T., Wolter A., 1991, ApJ, 274, 117
Metcalfe N., Shanks T., Fong R., Jones L.R., 1991, 249, 498
McMahon R. G. 1991 in Crampton,D. ed. The Space Distribution of Quasars, ASP Conf. Ser. 21, Astron. Soc. Pacif., San Francisco, p.129
Laor A., Fiore F., Elvis M., Wilkes B. and McDowell J., 1994, ApJ, 435, 611
Laor A., Fiore F., Elvis M., Wilkes B. and McDowell J., 1996, ApJ, *submitted*
Page M.J., Carerra F.J., Mittaz J.P.D., Mason K.O., Hasinger G., 1996, in Zimmermann H.U., Trümper J.E., Yorke H. eds, MPE Report 263, Röntgenstrahlung from the Universe, Max-Planck-Institute für Extraterrestrische Physik, Garching, p497
Schmidt M., Green, R. F., 1983, Ap.J., 269, 352
Shanks T., Georgantopoulos I., Stewart G.C., Pounds K.A., Boyle B.J., Griffiths R.E., 1991, Nat, 353, 315
Stocke J. T., Morris S. L., Gioia I. M., Maccacaro T., Schild R., Wolter A., Fleming T. A., Henry J. P., 1991, ApJS, 76, 813
Shastri P., Wilkes B.J., Elvis M., McDowell J.C. 1993, ApJ, 410, 29
Wilkes B.J., 1986, MNRAS, 218, 331
Wilkes B.J. 1982 PhD Thesis, University of Cambridge, England
Wilkes B.J., Elvis M., 1987, ApJ, 323, 243
Wilkes B.J., Wright A.E., Jauncey, D.L., Peterson B.A. 1983, Proc. ASA, 4, 3
Zamorani G. et al., 1981, ApJ, 245, 357

This paper has been produced using the Blackwell Scientific Publications TEX macros.